

# Chiral and deconfinement properties of the QCD crossover have a different volume and baryochemical potential dependence

Szabolcs Borsányi<sup>a</sup>, Zoltán Fodor<sup>a,b,c,d,e</sup>, Jana N. Guenther<sup>a</sup>, Ruben Kara<sup>a</sup>, Paolo Parotto<sup>f</sup>, Attila Pásztor<sup>c,g,†</sup>, Ludovica Pirelli<sup>a</sup>, Chik Him Wong<sup>a</sup>

<sup>a</sup> *Department of Physics, Wuppertal University, Gausstr. 20, D-42119, Wuppertal, Germany*

<sup>b</sup> *Pennsylvania State University, Department of Physics, State College, PA 16801, USA*

<sup>c</sup> *Institute for Theoretical Physics, ELTE Eötvös Loránd University,*

*Pázmány P. sétány 1/A, H-1117 Budapest, Hungary*

<sup>d</sup> *Jülich Supercomputing Centre, Forschungszentrum Jülich, D-52425 Jülich, Germany*

<sup>e</sup> *Physics Department, UCSD, San Diego, CA 92093, USA*

<sup>f</sup> *Dipartimento di Fisica, Università di Torino and INFN Torino, Via P. Giuria 1, I-10125 Torino, Italy*

<sup>g</sup> *HUN-REN-ELTE Theoretical Physics Research Group, Pázmány Péter sétány 1/A, H-1117 Budapest, Hungary*

(Dated: May 22, 2024)

The crossover from hadronic to quark matter is understood to be both a deconfinement as well as a chiral symmetry restoring transition. Here, we study observables related to both aspects using lattice simulations: the Polyakov loop and its derivatives and the chiral condensate and its derivatives. At zero baryochemical potential, and infinite volume, the chiral and deconfinement crossover temperatures almost agree. However, chiral and deconfinement related observables have a qualitatively different chemical potential and volume dependence. In general, deconfinement related observables have a milder volume dependence. Furthermore, while the deconfinement transition appears to get broader with increasing  $\mu_B$ , the width as well as the strength of the chiral transition is approximately constant. Our results are based on simulations at zero and imaginary chemical potentials using 4stout-improved staggered fermions with  $N_\tau = 12$  time-slices and physical quark masses.

## I. INTRODUCTION

The study of the phases of strongly interacting matter is an active field of research. In particular, the phase diagram in the temperature  $T$ -baryochemical potential  $\mu_B$  plane has garnered a lot of interest, both from the theoretical and experimental communities. First principle lattice QCD calculations have shown that the transition from a hadron gas to a quark-gluon plasma is a smooth crossover at zero and small chemical potentials [1]. At larger baryochemical potentials, model and functional calculations [2–5] predict the existence of a critical endpoint, where the crossover line in the  $T - \mu_B$  plane turns into a line of first order transitions. The position of this critical endpoint is very different in different model calculations. Thus, a first principle theory calculation, or an experimental discovery of its location, would be a great achievement. Indeed, the experimental discovery of this critical endpoint is one of the major goals of relativistic heavy ion physics [6].

First principle lattice QCD calculation at non-zero real  $\mu_B$  are hampered by a sign problem. Thus, most lattice results on physics at  $\mu_B > 0$  come from analytic continuation, either using lattice calculations of Taylor ex-

pansions around  $\mu_B = 0$  [7–16], or lattice calculations at purely imaginary chemical potentials [17–32]. While the ill-posedness of numerical analytic continuation limits the effectiveness of such methods, a lot has been learned by applying such methods to the study of the phase diagram at small enough  $\mu_B$ . Nevertheless, due to the ill-posed nature of numerical analytic continuation, such methods have a severe limitations. In particular, it is exceedingly difficult to reliably reach large chemical potentials with such methods.

A different set of methods is based on reweighting [33–44]. A subset of reweighting methods, sign and phase reweighting [39, 40, 43], have the advantage of giving more direct results. Thus, they have the advantage of better reliability, when compared to analytic continuation methods. However, they are, at least for the time being, restricted to smaller physical volumes, due to the high numerical costs. One motivation of this current work is to identify physical observables with milder finite volume effects, which can then later be calculated up to higher chemical potentials with such reweighting methods.

In this work, we use the imaginary chemical potential method to extrapolate certain physical observables

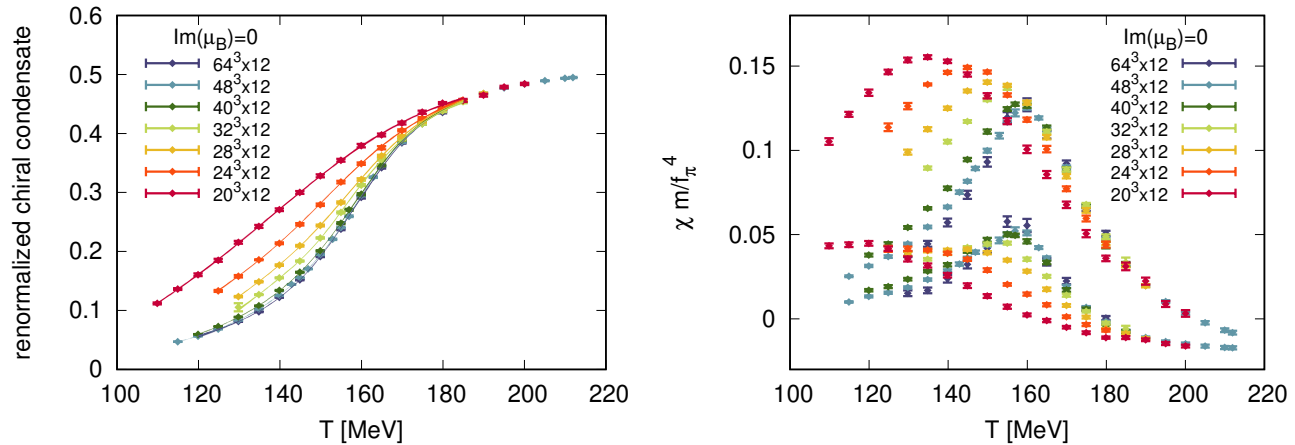


FIG. 1. Left panel: The renormalized chiral condensate (see eq. (5)) as a function of temperature for different spatial volumes. Right panel: The renormalized full and disconnected chiral susceptibility as a function of temperature for different spatial volumes.

to non-zero baryochemical potential  $\mu_B$ . We have two main goals. First, we want to compare observables related to the two main theoretical aspects of the QCD transition: chiral symmetry, which is an  $SU(2) \times SU(2)$  symmetry in the limit of light quarks, and confinement, which is related to a  $Z_3$  symmetry in the limit of heavy quarks. To study chiral dynamics, we will calculate the chiral condensate and chiral susceptibility. To study confinement/deconfinement mechanics we will calculate the Polyakov-loop and quantities derived from it: the static quark free energy and entropy. Second, we will look at the 3-volume dependence of the phase diagram. In particular, we will quantify the volume and  $\mu_B$  dependence of the crossover temperature, using different inequivalent definitions, based on both chiral symmetry and deconfinement, and calculate parameters defining the strength and width of the transition.

The picture we arrive at is nuanced. At infinite volume the crossover temperatures defined with the help of chiral symmetry and deconfinement are close, but not identical, and the volume dependence of the two crossover temperatures is different. The definition related to deconfinement has much smaller finite volume effects, and the sign of the finite volume effects is also the opposite: while the chiral crossover temperature increases with increasing volume, the deconfinement temperature decreases. The width and strength of the transition also behave differently. Again, quantities related to chiral symmetry show much larger finite volume effects. Furthermore, deconfinement related quantities show a weakening of the crossover transition with increasing  $\mu_B$ , both at small and large volumes. This is in contrast to chiral observables, which show a strengthening of the transition at smaller volumes and a roughly constant strength at large volumes.

The structure of the paper is as follows. First, we discuss the setup of our lattice simulations. Next, we discuss volume dependence at zero chemical potential. Then, we

go on to volume dependence at non-zero imaginary and real chemical potentials. We conclude with a summary and some speculations on the possible source of our findings.

## II. LATTICE SETUP

We use a tree-level Symanzik improved gauge action and four steps of stout smearing in the staggered fermion action, with  $N_f = 2 + 1 + 1$  flavours of dynamical quarks. The quark masses are tuned such that the pion and kaon masses are equal to 135 MeV and 495 MeV. The scale is set with the pion decay constant  $f_\pi = 130.41$  MeV. Details on the action, the scale setting and the line of constant physics can be found in Ref. [11]. We use lattices with  $N_\tau = 12$  timeslices. We use several physical volumes, with the number of spatial sites  $N_s = 20, 24, 28, 32, 40, 48$  and 64 for the  $\mu_B = 0$  simulations. For three of the spatial volumes ( $N_s = 32, 40$  and 48) we also simulate at a purely imaginary chemical potential, with  $\text{Im} \frac{\mu_B}{T} \frac{s}{\pi} = 3, 4, 5, 6, 6.5$  and 7. Throughout this work we always use a strangeness chemical potential  $\mu_S$  tuned in such a way that the expectation value of strangeness is equal to zero. This tuning of  $\mu_S$  is done to match conditions in heavy ion collisions, where the colliding nuclei in the initial state have zero strangeness. Details on setting the strangeness neutrality condition can be found in the supplemental material of Ref. [32]. In this work we only show statistical errors.

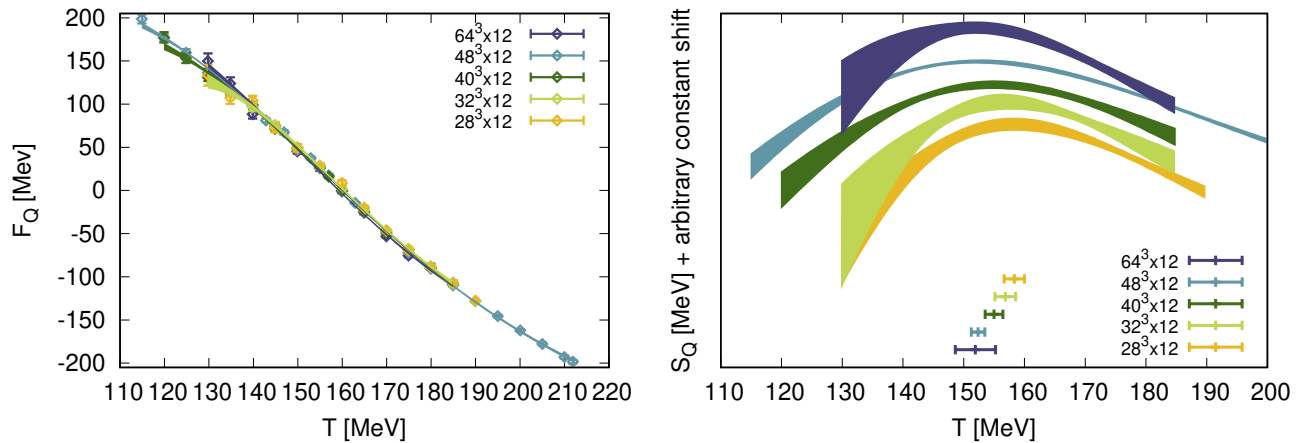


FIG. 2. Left panel: The static quark free energy (see eq. (6)) as a function of temperature for different spatial volumes. Right panel: The static quark entropy as a function of temperature for different spatial volumes. In order for the curves not to overlap, they were shifted by arbitrary amounts in the vertical direction.

### III. VANISHING CHEMICAL POTENTIAL

#### A. Chiral observables

In order to study the chiral aspects of the QCD crossover we will calculate the chiral condensate  $\langle\bar{\psi}\psi\rangle$  and the chiral susceptibility  $\chi$  defined respectively as:

$$\langle\bar{\psi}\psi\rangle = \frac{T}{V} \frac{\partial \log Z}{\partial m_{ud}}, \quad \chi = \frac{T}{V} \frac{\partial^2 \log Z}{\partial m_{ud}^2}. \quad (1)$$

In the limit of zero quark masses  $\langle\bar{\psi}\psi\rangle$  functions as the order parameter of the chiral phase transition. In terms of the discretized (massive) Dirac operator for the up and down quarks  $M_{ud}$ , the chiral condensate is written as:

$$\langle\bar{\psi}\psi\rangle = \frac{1}{2} \frac{T}{V} \langle \text{Tr} M_{ud}^{-1} \rangle, \quad (2)$$

where  $\langle \dots \rangle$  means taking an expectation value over the gauge fields and the factor  $\frac{1}{2}$  appears due to staggered rooting. In lattice language, the order parameter is then proportional to the trace  $\text{Tr} M_{ud}^{-1}$ . We will also study the disconnected part of the chiral susceptibility, defined as:

$$\chi_{\text{disc}} = \frac{1}{4} \frac{T}{V} \left( \langle (\text{Tr} M_{ud}^{-1})^2 \rangle - \langle \text{Tr} M_{ud}^{-1} \rangle^2 \right), \quad (3)$$

where the factor of 1/4 is present - again - due to staggered rooting. This is essentially the variance of  $\text{Tr} M_{ud}^{-1}$  in the lattice QCD language. The disconnected susceptibility can also be defined as a cross-derivative:

$$\chi_{\text{disc}} = \frac{T}{V} \left( \frac{\partial^2}{\partial m_u \partial m_d} \log Z \right)_{m_u=m_d}, \quad (4)$$

thus, it is a legitimate physical observable. We study both the full and disconnected susceptibilities, because

they may be sensitive in different ways to the distinct critical points present in the 3 dimensional QCD phase diagram spanned by the variables  $T$ ,  $\mu_B^2$  and  $m_{ud}$ .

The condensate and the susceptibilities contain both multiplicative and additive UV divergences. One possible definition of UV finite condensate and susceptibility is given by the following renormalization prescription:

$$\begin{aligned} \langle\bar{\psi}\psi\rangle^R &= -\frac{m_{ud}}{f_\pi^4} [\langle\bar{\psi}\psi\rangle_T - \langle\bar{\psi}\psi\rangle_{T=0}], \\ \chi^R &= \frac{m_{ud}^2}{f_\pi^4} [\chi_T - \chi_{T=0}], \\ \chi_{\text{disc}}^R &= \frac{m_{ud}^2}{f_\pi^4} [\chi_{\text{disc},T} - \chi_{\text{disc},T=0}], \end{aligned} \quad (5)$$

where the division by  $f_\pi^4$  is there to ensure the quantities  $\langle\bar{\psi}\psi\rangle^R$ ,  $\chi^R$  and  $\chi_{\text{disc}}^R$  are dimensionless.

The peak position of either the full or disconnected susceptibilities can be used to define the chiral crossover temperature. Similarly, the maximal value of either of these susceptibilities can be used to study the strength of the crossover transition, as they both diverge in the presence of true critical behavior.

The lattice results for the chiral condensate as well as the full and disconnected susceptibilities as functions of the temperature are shown in Fig. 1 for several lattice volumes.

At zero temperature, chiral perturbation theory predicts [45] the condensate to have finite volume effects of the form  $\propto A e^{-m_\pi L} L^{-3/2}$ . We have checked that this ansatz describes our data for temperatures  $T \leq 150 \text{ MeV}$  [46]. The prefactor  $A$  is related to the chiral condensate in the chiral limit, i.e., to the topological susceptibility - according to the Leutwyler-Smilga relation [47] - which is known to have very large cut-off effects with staggered fermions. We will thus not present it here, from these  $N_\tau = 12$  lattices.

The left panel of Fig. 1 shows the temperature dependence of the chiral condensate for different volumes, while the right panel shows the temperature dependence of both the full and disconnected susceptibilities. While there are strong volume effects, both the slope of the condensate and the maximum value of the susceptibility converges to a finite value at large volume, consistent with a crossover. We clearly see that the finite volume effects on both the condensate and the two susceptibilities decrease with increasing temperature. This can intuitively be understood, because the screening mass of the pseudoscalar channel (i.e., the smallest of the screening masses) is increasing at temperatures above the crossover transition, or equivalently, the largest spatial correlation length relevant for the finite volume effects is decreasing.

Near the transition temperature, both the full and disconnected susceptibilities show a behavior that is characteristic of a crossover transition: their maximal value tends to a finite number in the thermodynamic limit. Later in this manuscript, we will study the chemical potential dependence of this maximal value, to infer whether the crossover transition gets stronger with increasing chemical potential, i.e., in some sense closer to a second order transition, as expected in the presence of a critical endpoint.

## B. Deconfinement observables

We now look at properties of static test quarks, which is a common way to characterize confinement.

The static quark free energy [48]  $F_Q$  and the static quark entropy  $S_Q$  are defined as [49] [50]:

$$F_Q = -T \log \left( \frac{1}{V} \sum_{\vec{x}} |\langle P(\vec{x}) \rangle_T| \right) + T_0 \log \left( \frac{1}{V} \sum_{\vec{x}} |\langle P(\vec{x}) \rangle_{T_0}| \right), \quad (6)$$

$$S_Q = -\frac{\partial F_Q}{\partial T},$$

where  $P(\vec{x})$  is the Polyakov loop

$$P(\vec{x}) = \frac{1}{3} \text{Tr} \prod_{x_4=0}^{N_t-1} U_4(\vec{x}, x_4), \quad (7)$$

the  $U_\mu(\vec{x}, x_4)$  are the usual link variables in lattice gauge theory,  $T_0$  is a reference temperature, and the second term in the definition of  $F_Q$  is needed to remove the additive divergence in the free energy. The value of the reference temperature  $T_0$ , together with Eq. (6) defines a renormalization scheme for the static quark free energy. The subtraction has to be done at the same value of the lattice spacing. The quantity  $F_Q$  is then a UV finite quantity, with a well defined continuum limit. Note that taking the absolute value of the (complex) Polyakov

loop expectation value in Eq. (6) is not important at vanishing or real chemical potential, as in both cases this expectation value is real. We include it in the formula, in order to keep the same definition for arbitrary complex chemical potential, including a purely imaginary chemical potential, where the expectation value is no longer real and the absolute value is needed. The entropy  $S_Q$  is estimated by interpolating the lattice results for  $F_Q(T)$  and differentiating the interpolating function. For the interpolation we use a 2nd order-by-2nd order rational function fit. The chi squares of all of the fits in  $T$  are acceptable.

For pure gauge theory, where a true first order deconfinement phase transition is present, the static quark free energy is infinite in the confined phase (i.e., the Polyakov loop is zero). For full QCD, this is no longer the case. Nevertheless, one can use the peak of  $S_Q(T)$  (the inflection point of  $F_Q(T)$ ) to define a crossover temperature. In the limit of infinitely heavy quarks, the peak position of  $S_Q(T)$  coincides with the deconfinement phase transition temperature. The height of the peak of  $S_Q(T)$  is inversely proportional to the thermal width of the deconfinement crossover. Our results for  $F_Q(T)$  and  $S_Q(T)$  are shown in Fig. 2 for several different spatial volumes.

We note that a different observable was used to define the confinement crossover temperature in Ref. [51], where the authors introduced the susceptibility  $\chi_{Q,\mu_B^2} \equiv -\left(\frac{\partial(F_Q/T)}{\partial(\mu_B/T)^2}\right)_{\mu_B=0}$ , which also shows a peak at the crossover transition. We, however, have found that we get statistically more precise results for  $S_Q$ , and therefore use this quantity to define the deconfinement crossover temperature in what follows.

We are now in a position to compare the deconfinement and chiral symmetry related definitions of the crossover temperature. We show the different values of  $T_c$  defined as the peak of  $\chi^R(T)$ , the peak of  $\chi_{disc}^R(T)$  as well as the peak of  $S_Q(T)$  in Fig. 3. For comparison, we also show a curve where the chiral condensate, or the static quark free energy is constant, with the constant chosen to be the infinite volume value at the crossover temperature defined via the full chiral susceptibility.

Fig. 3 establishes an ordering of the different crossover temperatures in the infinite volume limit:

$$T_c^{(S_Q)} < T_c^{(\chi_{disc}^R)} < T_c^{\chi^R}. \quad (8)$$

The differences between definitions are small, amounting only to a few MeV. The identification of such an ordering had never been possible in existing literature, due to larger error bars. Thus, our work is an improvement on previous work in Ref. [50] where the chiral and deconfinement transition temperatures were in agreement within errorbars. Furthermore, we see a different volume dependence of the different crossover temperatures. Namely, the two chiral definitions lead to a  $T_c$  that is monotonically increasing with the physical volume, while the deconfinement definition leads to a  $T_c$  that is monotonically decreasing with the volume. This means that at

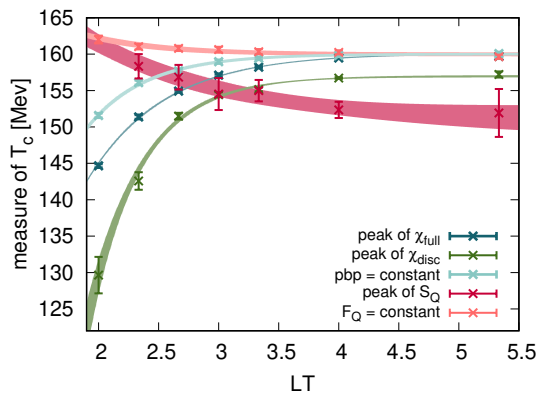


FIG. 3. Five different definitions of the transition temperature as functions of the simulation volume, labeled by the aspect ratio  $LT = N_x/N_t$ . The blue and green points refer to the peak position of the full and disconnected chiral susceptibility, respectively. In addition, we show the temperature where the chiral condensate is constant (light blue). In all cases, the infinite volume value is approached from below. The two other measures of  $T_c$  come from the Polyakov loop, either keeping a constant value for  $F_Q$  (pink), or determining the maximum of the static quark entropy  $S_Q$  (purple). In both cases, the infinite volume value is approached from above. The fixed values of the chiral condensate and  $F_Q$  have been set such that these match the infinite volume limit at the maximum of the full chiral susceptibility.

small enough volumes, the ordering changes, and the definition of  $T_c$  based on the static quark entropy becomes the largest. We also note that finite volume effects on the deconfinement based definition of  $T_c$  appear to be smaller. Even on the smallest lattice, with aspect ratio  $LT = 2$ , the deconfinement based definition gives a results of around 160MeV, which is quite close to the infinite volume value, and is much larger than the chiral symmetry based definitions.

#### IV. NON-VANISHING CHEMICAL POTENTIAL

We now go on to discuss the phase diagram for  $\mu_B > 0$ . First, we briefly explain the analysis method, then we discuss the phase diagram, that is the volume and chemical potential dependence of the crossover temperature, and finally, the volume and chemical potential dependence of the strength and width of the crossover transition. We will use the same quantities that we used in the  $\mu_B = 0$  analysis.

##### A. Observables at imaginary chemical potential

Our extrapolation method to real baryochemical potential is based on the observation of an approximate data collapse [32]. The chiral susceptibility as a function of the chiral condensate is a curve that is almost inde-

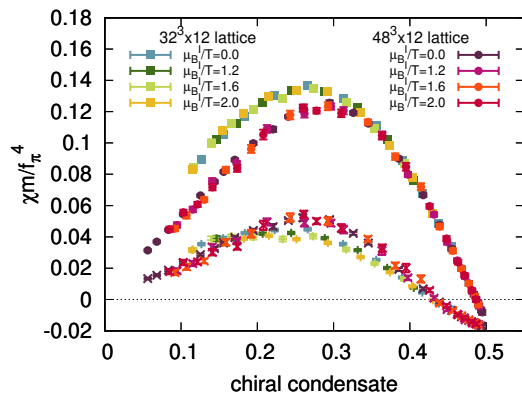


FIG. 4. The full (filled symbols) and disconnected (crosses) chiral susceptibilities as a function of the condensate for two different volumes and several values of the imaginary chemical potential.

pendent of the imaginary chemical potential. In Ref. [32] we demonstrated this for the full susceptibility. Here, we show it both for  $\chi_{full}$  and  $\chi_{disc}$  in Fig. 4 where both susceptibilities are shown as functions of the condensate for several imaginary chemical potentials, for two different volumes. While the collapse curves for both susceptibilities are approximately independent of the imaginary chemical potential, they significantly depend on the volume. Also note that the susceptibilities as functions of the condensate are considerably simpler functions than the susceptibilities as functions of the temperature, in the sense that they are well described by low order polynomials.

In light of this collapse, the extraction of the crossover temperature follows the following steps:

1. determine the renormalized (full or disconnected) susceptibility as a function of the condensate for several values of the imaginary baryochemical potential;
2. find the peak position in the susceptibility as a function of the condensate for each value of  $\text{Im } \mu_B/T$  with a low order polynomial fit;
3. use an interpolation of the condensate as a function of  $T$  to convert the peak position from the condensate value to the temperature for each  $\text{Im } \mu_B/T$ ;
4. perform a fit of  $T_c(\text{Im } \mu_B/T_c)$ , and use the fit to extrapolate the crossover temperature from  $\mu_B^2 \leq 0$  to  $\mu_B^2 > 0$ .

We note that this extrapolation method was also cross-checked in a calculation with truncated Dyson-Schwinger equations, where the approximation allows for direct calculations at  $\mu_B > 0$ . The authors of Ref. [52] found good agreement between the direct calculations and the extrapolated results.

If instead of the chiral condensate, one attempts to show the chiral susceptibility as a function of the static

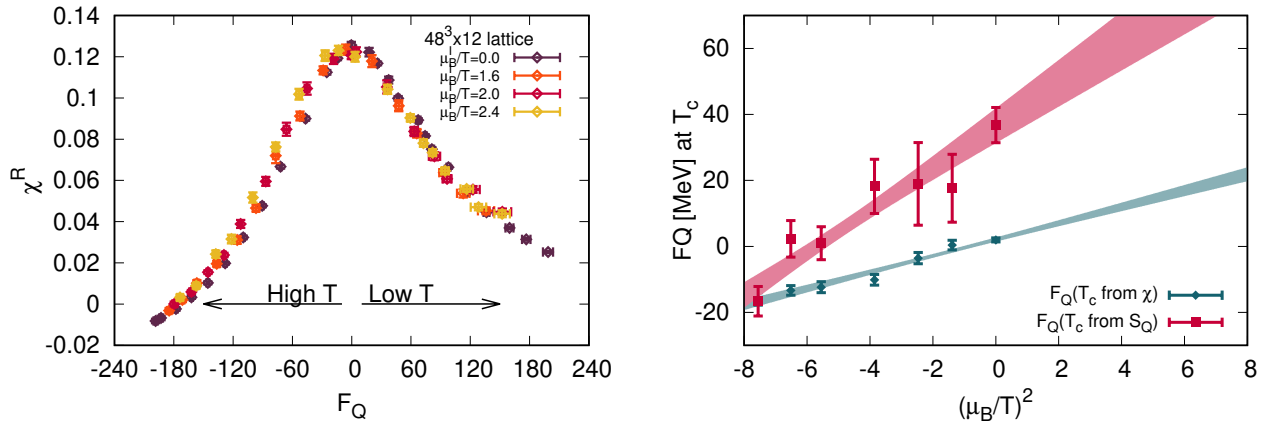


FIG. 5. Left: The full chiral susceptibility as a function of the static quark free energy. Right: The value of  $F_Q$  at the chiral crossover temperature (defined via the peak of the full chiral susceptibility or the static quark entropy) as a function of  $\mu_B^2/T^2$ . A linear extrapolation is also shown.

quark free energy  $F_Q$ , the collapse is less accurate. This is shown in Fig. 5, where the left panel shows  $\chi_{full}$  as a function of  $F_Q$  for several imaginary chemical potentials on our  $48^3 \times 12$  lattices. To quantify the inaccuracy of the collapse plot we show the value of  $F_Q$  at the crossover temperature (defined either via  $\chi_{full}$  or of  $S_Q$ ) as a function of  $\mu_B^2/T^2$  in the right panel of the same figure, where a linear extrapolation of the value of  $F_Q$  at the crossover temperature is also shown. While it is not shown in the plot, to avoid clutter, we note that the disconnected susceptibility also has a similar (non-perfect) collapse feature as a function of  $F_Q$ .

For the calculation of the crossover temperature defined with  $S_Q$ , we simply use the same rational function fit of  $F_Q(T)$  that we used for the  $\mu_B = 0$  case.

### B. The phase diagram for real $\mu_B > 0$

We are now in a position to discuss the volume dependence of the phase diagram. We show the crossover temperature, defined via the peak position of the full and disconnected chiral condensates, as well as the static quark entropy as a function of  $\mu_B^2/T^2$  in the left panel of Fig. 6 in a fixed volume, on our  $48^3 \times 12$  lattices. We see that not only  $T_c(\mu_B = 0)$ , but also the chemical potential dependence is different for the different definitions. At larger imaginary chemical potentials, the three definitions come closer to each other, which might be due to the presence of the Roberge-Weiss critical endpoint. In the near vicinity of such a critical point, the crossover transition should get narrower, and we thus expect different definitions of the crossover temperature to converge towards each other. This is exactly what we observe.

Here, we note that in the strangeness neutral setting employed in the present paper, the Roberge-Weiss transition is not located at  $\text{Im} \mu_B/T = \pi$ , but at a slightly

larger value [53].

We also show contours of constant values of the static quark free energy and the chiral condensate for two different 3-volumes in the  $T - \mu_B^2$  plane in Fig. 7. It is apparent that  $F_Q$  has much milder finite volume effects than the chiral condensate, especially at imaginary chemical potentials  $\mu_B < 0$ . This is somewhat surprising, since at imaginary chemical potentials, one might expect  $F_Q$  to have strong finite-volume effects, being closely related to the Polyakov loop, which is the order parameter for the Roberge-Weiss transition at imaginary chemical potentials.

### C. The strength of the crossover for real $\mu_B \neq 0$

A very interesting question, with more phenomenological implications, is whether the crossover line turns into a line of first order transitions at a critical endpoint at some real value of the baryochemical potential  $\mu_B$ . If it does, it is expected that the crossover transition becomes narrower and stronger at larger  $\mu_B$ , at least in the vicinity of the critical endpoint. Here, we discuss some measures of the width or strength of the transition as a function of  $\mu_B$  for small chemical potentials.

In Fig. 8 we show the values of  $S_Q$ ,  $\chi^R$  and  $\chi_{disc}^R$  at the crossover temperature as functions of  $\mu_B^2/T^2$ , for two different physical 3-volumes. The points with error bars are our direct lattice results at zero and purely imaginary chemical potentials, while the bands show linear extrapolations in  $\mu_B^2/T^2$ . All three quantities should diverge at the critical endpoint in the infinite volume limit. Thus, with increasing volume, one expects these quantities to grow in the vicinity of the critical endpoint. The only one of these quantities showing a rise at larger  $\mu_B^2$  is  $\chi_{disc}^R$ , while  $\chi^R$  remains approximately constant up to our largest volume, and  $S_Q$  decreases with increasing  $\mu_B^2$ .

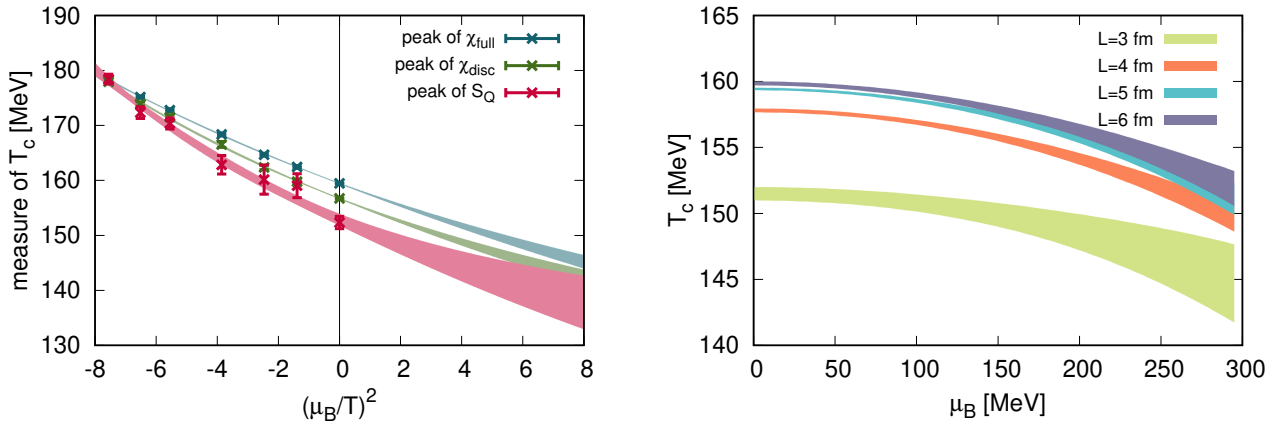


FIG. 6. Left panel: extrapolation of the crossover temperature as a function of  $\mu_B^2/T^2$  using the three different definitions discussed in the main text on our  $48^3 \times 12$  lattices. Right panel: Crossover temperature defined via the peak of  $\chi_{full}$  for different lattice volumes, fixed in fermis.

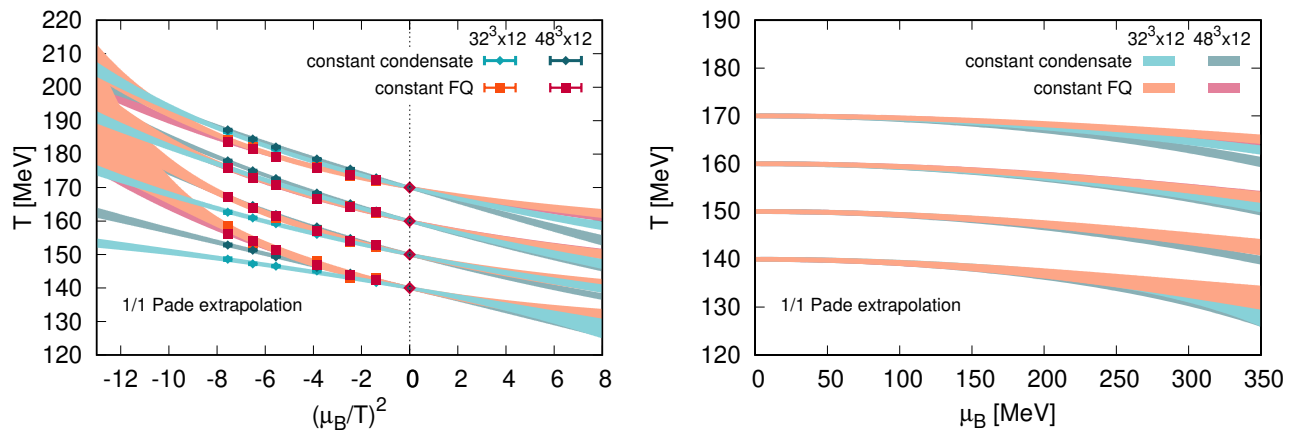


FIG. 7. Extrapolated contours with a constant value of the static quark free energy  $F_Q$  and the renormalized chiral condensate  $\langle \bar{\psi}\psi \rangle^R$  in the  $T - \mu_B^2$  plane (left) and in the  $T - \mu_B$  plane (right) for two different volumes.

From the behavior of  $\chi_{disc}^R$  alone, one might be tempted to conclude that the crossover transition gets stronger at larger  $\mu_B$ , which would be a signal of the coveted critical endpoint. However, the lack of a similar behavior in the other two quantities -  $S_Q$  and  $\chi^R$  makes the interpretation of the physical picture uncertain.

Furthermore, we once again see that the deconfinement related quantity ( $S_Q$ ) has milder finite volume effects than the quantities related to chiral symmetry restoration ( $\chi^R$  and  $\chi_{disc}^R$ ). Just like in the case of  $F_Q$  above, the small volume dependence of  $S_Q$  at imaginary chemical potentials is surprising, since one expects large finite volume effects due to the Roberge-Weiss endpoint. Apparently the imaginary chemical potentials considered in our study are not close enough to the Roberge-Weiss critical endpoint for this to be the case.

The disconnected susceptibility shows the most interesting behavior: an increasing trend with increasing  $\mu_B^2$ ,

especially for the two lower volumes. If the coveted QCD critical endpoint exists, such a behavior could be due to the critical region shrinking with increasing physical volume. (I.e., a smaller volume is more tolerant to the mistuning of the parameters of a system, and criticality can be observed from farther away.) Due to the lack of such a signal in  $\chi^R$  and  $S_Q$ , we would be cautious about making such an interpretation, but the behavior of  $\chi_{disc}^R$  certainly is suggestive and warrants further investigation.

## V. DISCUSSION

In this work we investigated the volume and chemical potential dependence of the location and the strength of the QCD transition, by studying observables related to either deconfinement or chiral symmetry restoration.

At vanishing chemical potential, we found - in the ther-

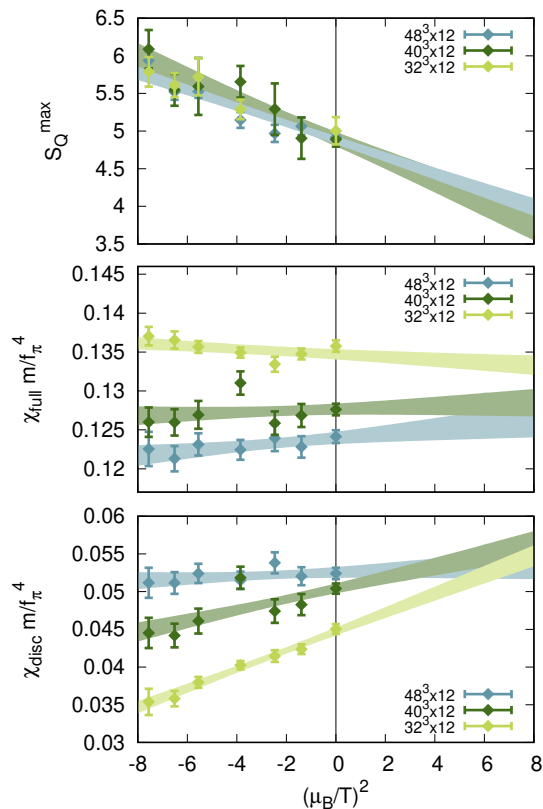


FIG. 8. Extrapolation of the maximal value of the full and disconnected chiral susceptibilities as a function of  $\mu_B^2/T^2$  for three different volumes.

modynamic limit - the following ordering of the crossover temperatures:  $T_c^{(S_Q)} < T_c^{(\chi_{disc}^R)} < T_c^{(\chi^R)}$ . Hence, we found the deconfinement crossover temperatures to be slightly below the chiral crossover temperature. Furthermore, we found that the deconfinement crossover temperature and the chiral crossover temperatures have a different sign for their volume dependence. While with increasing volume  $T_c^{(S_Q)}$  decreases,  $T_c^{(\chi_{disc}^R)}$  and  $T_c^{(\chi^R)}$  both increase.

Curves of constant heavy quark free energy (related to

confinement) and constant chiral condensate (related to chiral symmetry breaking) in the  $T - \mu_B^2/T^2$  plane are similar, but not identical. In particular, the curvature of these lines is about the same at  $T_c(\mu_B = 0)$ , but not below or above.

In general, we find that physical quantities related to confinement dynamics appear to have much milder finite volume effects, when compared to quantities related to chiral symmetry. This is true at both zero and non-zero baryochemical potential, be it imaginary (simulated) or real (extrapolated). Thus, confinement-deconfinement mechanics will be easier to study in settings where larger volumes are too expensive, which is the case, e.g., with reweighting techniques.

Finally, we found that the volume and  $\mu_B$  dependence of the maximal value of  $\chi^R$ ,  $\chi_{disc}^R$  and  $S_Q$  are non-trivial, and a clear physical picture cannot be drawn at the moment. However, the disconnected susceptibility  $\chi_{disc}^R$  in particular shows suggestive behavior, which is promising in light of future theoretical searches for the QCD critical point.

#### ACKNOWLEDGEMENTS

The project was supported by the BMBF Grant No. 05P21PXFCA. This work is also supported by the MKW NRW under the funding code NW21-024-A. Further funding was received from the DFG under the Project No. 496127839. This work was also supported by the Hungarian National Research, Development and Innovation Office, NKFIH Grant No. KKP126769. This work was also supported by the NKFIH excellence grant TKP2021\_NKTA\_64. The project was also supported by the Hungarian National Research, Development and Innovation Office under Project No. FK 147164. The authors gratefully acknowledge the Gauss Centre for Supercomputing e.V. ([www.gauss-centre.eu](http://www.gauss-centre.eu)) for funding this project by providing computing time on the GCS Supercomputers Juwels-Booster at Juelich Supercomputer Centre and HAWK at Höchstleistungsrechenzentrum Stuttgart.

- [1] Y. Aoki, G. Endrodi, Z. Fodor, S.D. Katz, and K.K. Szabo. The Order of the quantum chromodynamics transition predicted by the standard model of particle physics. *Nature*, 443:675–678, 2006.
- [2] Peter Kovács, Zsolt Szép, and György Wolf. Existence of the critical endpoint in the vector meson extended linear sigma model. *Phys. Rev. D*, 93(11):114014, 2016.
- [3] Fei Gao and Jan M. Pawłowski. QCD phase structure from functional methods. *Phys. Rev. D*, 102(3):034027, 2020.
- [4] Wei-jie Fu, Xiaofeng Luo, Jan M. Pawłowski, Fabian Rennecke, Rui Wen, and Shi Yin. Hyper-order baryon

number fluctuations at finite temperature and density. *Phys. Rev. D*, 104(9):094047, 2021.

- [5] Philipp Isserstedt, Michael Buballa, Christian S. Fischer, and Pascal J. Gunkel. Baryon number fluctuations in the QCD phase diagram from Dyson-Schwinger equations. *Phys. Rev.*, D100(7):074011, 2019.
- [6] J. Adam et al. Nonmonotonic Energy Dependence of Net-Proton Number Fluctuations. *Phys. Rev. Lett.*, 126(9):092301, 2021.
- [7] Rajiv V. Gavai and Sourendu Gupta. Pressure and non-linear susceptibilities in QCD at finite chemical potentials. *Phys.Rev.*, D68:034506, 2003.



- [8] C.R. Allton, M. Doring, S. Ejiri, S.J. Hands, O. Kaczmarek, et al. Thermodynamics of two flavor QCD to sixth order in quark chemical potential. *Phys.Rev.*, D71:054508, 2005.
- [9] Szabolcs Borsanyi, Zoltan Fodor, Sandor D. Katz, Stefan Krieg, Claudia Ratti, et al. Fluctuations of conserved charges at finite temperature from lattice QCD. *JHEP*, 1201:138, 2012.
- [10] Sz. Borsanyi, G. Endrodi, Z. Fodor, S.D. Katz, S. Krieg, et al. QCD equation of state at nonzero chemical potential: continuum results with physical quark masses at order  $mu^2$ . *JHEP*, 1208:053, 2012.
- [11] R. Bellwied, S. Borsanyi, Z. Fodor, S. D. Katz, A. Pasztor, C. Ratti, and K. K. Szabo. Fluctuations and correlations in high temperature QCD. *Phys. Rev.*, D92(11):114505, 2015.
- [12] H. T. Ding, Swagato Mukherjee, H. Ohno, P. Petreczky, and H. P. Schadler. Diagonal and off-diagonal quark number susceptibilities at high temperatures. *Phys. Rev.*, D92(7):074043, 2015.
- [13] A. Bazavov et al. The QCD Equation of State to  $\mathcal{O}(\mu_B^6)$  from Lattice QCD. *Phys. Rev.*, D95(5):054504, 2017.
- [14] A. Bazavov et al. Chiral crossover in QCD at zero and non-zero chemical potentials. *Physics Letters B*, 795:15–21, Aug 2019.
- [15] Matteo Giordano and Attila Pasztor. Reliable estimation of the radius of convergence in finite density QCD. *Phys. Rev.*, D99(11):114510, 2019.
- [16] A. Bazavov et al. Skewness, kurtosis and the 5th and 6th order cumulants of net baryon-number distributions from lattice QCD confront high-statistics STAR data. *Physical Review D*, 101(7), Apr 2020.
- [17] Philippe de Forcrand and Owe Philipsen. The QCD phase diagram for small densities from imaginary chemical potential. *Nucl. Phys.*, B642:290–306, 2002.
- [18] Massimo D’Elia and Maria-Paola Lombardo. Finite density QCD via imaginary chemical potential. *Phys. Rev.*, D67:014505, 2003.
- [19] Massimo D’Elia and Francesco Sanfilippo. Thermodynamics of two flavor QCD from imaginary chemical potentials. *Phys. Rev.*, D80:014502, 2009.
- [20] Paolo Cea, Leonardo Cosmai, and Alessandro Papa. Critical line of 2+1 flavor QCD. *Phys. Rev.*, D89(7):074512, 2014.
- [21] Claudio Bonati, Philippe de Forcrand, Massimo D’Elia, Owe Philipsen, and Francesco Sanfilippo. The chiral phase transition in two-flavor QCD from imaginary chemical potential. *Physical Review D*, 90(7), Oct 2014.
- [22] Paolo Cea, Leonardo Cosmai, and Alessandro Papa. Critical line of 2+1 flavor QCD: Toward the continuum limit. *Phys. Rev.*, D93(1):014507, 2016.
- [23] Claudio Bonati, Massimo D’Elia, Marco Mariti, Michele Mesiti, Francesco Negro, and Francesco Sanfilippo. Curvature of the chiral pseudocritical line in QCD: Continuum extrapolated results. *Phys. Rev.*, D92(5):054503, 2015.
- [24] R. Bellwied, S. Borsanyi, Z. Fodor, J. Günther, S. D. Katz, C. Ratti, and K. K. Szabo. The QCD phase diagram from analytic continuation. *Phys. Lett.*, B751:559–564, 2015.
- [25] Massimo D’Elia, Giuseppe Gagliardi, and Francesco Sanfilippo. Higher order quark number fluctuations via imaginary chemical potentials in  $N_f = 2+1$  QCD. *Phys. Rev.*, D95(9):094503, 2017.
- [26] J. Gunther, R. Bellwied, S. Borsanyi, Z. Fodor, S. D. Katz, A. Pasztor, and C. Ratti. The QCD equation of state at finite density from analytical continuation. *EPJ Web Conf.*, 137:07008, 2017.
- [27] Paolo Alba et al. Constraining the hadronic spectrum through QCD thermodynamics on the lattice. *Phys. Rev.*, D96(3):034517, 2017.
- [28] Volodymyr Vovchenko, Attila Pasztor, Zoltan Fodor, Sandor D. Katz, and Horst Stoecker. Repulsive baryonic interactions and lattice QCD observables at imaginary chemical potential. *Phys. Lett.*, B775:71–78, 2017.
- [29] Claudio Bonati, Massimo D’Elia, Francesco Negro, Francesco Sanfilippo, and Kevin Zambello. Curvature of the pseudocritical line in QCD: Taylor expansion matches analytic continuation. *Phys. Rev.*, D98(5):054510, 2018.
- [30] Szabolcs Borsanyi, Zoltan Fodor, Jana N. Guenther, Sandor K. Katz, Kalman K. Szabo, Attila Pasztor, Israel Portillo, and Claudia Ratti. Higher order fluctuations and correlations of conserved charges from lattice QCD. *JHEP*, 10:205, 2018.
- [31] Rene Bellwied, Szabolcs Borsanyi, Zoltan Fodor, Jana N. Guenther, Jacquelyn Noronha-Hostler, Paolo Parotto, Attila Pasztor, Claudia Ratti, and Jamie M. Stafford. Off-diagonal correlators of conserved charges from lattice QCD and experiment. *Physical Review D*, 101(3), Feb 2020.
- [32] Szabolcs Borsanyi, Zoltan Fodor, Jana N. Guenther, Ruben Kara, Sandor D. Katz, Paolo Parotto, Attila Pasztor, Claudia Ratti, and Kalman K. Szabo. The QCD crossover at finite chemical potential from lattice simulations. *Phys. Rev. Lett.*, 125:052001, 2020.
- [33] Ian M. Barbour, Susan E. Morrison, Elyakum G. Klepfish, John B. Kogut, and Maria-Paola Lombardo. Results on finite density QCD. *Nucl. Phys. Proc. Suppl.*, 60A:220–234, 1998. [220(1997)].
- [34] Z. Fodor and S.D. Katz. A New method to study lattice QCD at finite temperature and chemical potential. *Phys.Lett.*, B534:87–92, 2002.
- [35] Z. Fodor and S.D. Katz. Lattice determination of the critical point of QCD at finite T and mu. *JHEP*, 0203:014, 2002.
- [36] Z. Fodor and S.D. Katz. Critical point of QCD at finite T and mu, lattice results for physical quark masses. *JHEP*, 0404:050, 2004.
- [37] P. de Forcrand, S. Kim, and T. Takaishi. QCD simulations at small chemical potential. *Nucl. Phys. B Proc. Suppl.*, 119:541–543, 2003.
- [38] Andrei Alexandru, Manfred Faber, Ivan Horvath, and Keh-Fei Liu. Lattice QCD at finite density via a new canonical approach. *Phys. Rev.*, D72:114513, 2005.
- [39] Matteo Giordano, Kornel Kapas, Sandor D. Katz, Daniel Negradi, and Attila Pasztor. New approach to lattice QCD at finite density; results for the critical end point on coarse lattices. *JHEP*, 05:088, 2020.
- [40] Szabolcs Borsanyi, Zoltan Fodor, Matteo Giordano, Sandor D. Katz, Daniel Negradi, Attila Pasztor, and Chik Him Wong. Lattice simulations of the QCD chiral transition at real baryon density. *Phys. Rev. D*, 105(5):L051506, 2022.
- [41] Zoltan Fodor, Sandor D. Katz, and Christian Schmidt. The Density of states method at non-zero chemical potential. *JHEP*, 0703:121, 2007.
- [42] G. Endrodi, Z. Fodor, S. D. Katz, D. Sexty, K. K. Szabo, and Cs. Torok. Applying constrained simulations for

- low temperature lattice QCD at finite baryon chemical potential. *Phys. Rev.*, D98(7):074508, 2018.
- [43] Szabolcs Borsanyi, Zoltan Fodor, Matteo Giordano, Jana N. Guenther, Sandor D. Katz, Attila Pasztor, and Chik Him Wong. Equation of state of a hot-and-dense quark gluon plasma: Lattice simulations at real  $\mu_B$  vs extrapolations. *Phys. Rev. D*, 107(9):L091503, 2023.
- [44] Szabolcs Borsanyi, Zoltan Fodor, Matteo Giordano, Jana N. Guenther, Sandor D. Katz, Attila Pasztor, and Chik Him Wong. Can rooted staggered fermions describe nonzero baryon density at low temperatures? 8 2023.
- [45] P. Gerber and H. Leutwyler. Hadrons Below the Chiral Phase Transition. *Nucl.Phys.*, B321:387, 1989.
- [46] Szabolcs Borsányi, Zoltán Fodor, Jana N. Guenther, Ruben Kara, Paolo Parotto, Attila Pásztor, and Chik Him Wong. Finite volume effects near the chiral crossover. 1 2024.
- [47] H. Leutwyler and Andrei V. Smilga. Spectrum of Dirac operator and role of winding number in QCD. *Phys. Rev.*, D46:5607–5632, 1992.
- [48] Larry D. McLerran and Benjamin Svetitsky. Quark Liberation at High Temperature: A Monte Carlo Study of SU(2) Gauge Theory. *Phys. Rev. D*, 24:450, 1981.
- [49] More precisely, it is the excess free energy from inserting a static test quark in the medium.
- [50] A. Bazavov, N. Brambilla, H. T. Ding, P. Petreczky, H. P. Schadler, A. Vairo, and J. H. Weber. Polyakov loop in 2+1 flavor QCD from low to high temperatures. *Phys. Rev.*, D93(11):114502, 2016.
- [51] Massimo D’Elia, Francesco Negro, Andrea Rucci, and Francesco Sanfilippo. Dependence of the static quark free energy on  $\mu_B$  and the crossover temperature of  $N_f = 2+1$  QCD. *Phys. Rev. D*, 100(5):054504, 2019.
- [52] Julian Bernhardt and Christian S. Fischer. From imaginary to real chemical potential QCD with functional methods. *Eur. Phys. J. A*, 59(8):181, 2023.
- [53] Claudio Bonati, Massimo D’Elia, Marco Mariti, Michele Mesiti, Francesco Negro, et al. Curvature of the chiral pseudocritical line in QCD. *Phys.Rev.*, D90(11):114025, 2014.